Large scale magnetic fields and the number of cosmic ray sources above the Greisen-Zatsepin-Kuzmin cutoff

Claudia Isola, Günter Sigl

Large scale magnetic fields and the number of cosmic ray sources above the Greisen-Zatsepin-Kuzmin cutoff

Claudia Isola
Centre de Physique Théorique, Ecole Polytechnique, 91128 Palaiseau Cedex, France
and GReCO, Institut d'Astrophysique de Paris, C.N.R.S., 98 bis boulevard Arago, F-75014 Paris, France

Günter Sigl
GReCO, Institut d'Astrophysique de Paris, C.N.R.S., 98 bis boulevard Arago, F-75014 Paris, France
(Received 18 March 2002; published 10 October 2002)

We present numerical simulations for the two-point correlation function and the angular power spectrum of nucleons above 10^{19} eV injected by a discrete distribution of continuously emitting sources which follow a simple approximation to the profile of the Local Supercluster. We develop a method to constrain the number of sources necessary to reproduce the observed sky distribution of ultrahigh energy cosmic rays, as a function of the strength of the large scale cosmic magnetic fields in the Local Supercluster. While for fields $B \lesssim 0.05\ \mu$G the Supercluster source distribution appears inconsistent with the data for any number of sources, fields of strength $B \simeq 0.3\ \mu$G could reproduce the observed data with a number of sources around 10.

DOI: 10.1103/PhysRevD.66.083002 PACS number(s): 98.70.Sa, 13.85.Tp, 98.54.Cm

I. INTRODUCTION

Despite a growing amount of data the origin of cosmic rays especially at the highest energies is still obscure. For ultrahigh energy cosmic rays (UHECR) with energies above 10^{18}, there are still many open questions such as ''How can particles be accelerated to these extremely high energies?,'' and ''What are their sources?'' [1]. The best candidates for acceleration sources are powerful objects, such as hot spots of radio galaxies and active galactic nuclei [2], but they are still not identified and it is still unknown how many of them contribute to the observed cosmic ray flux.

The observed spectrum covers about 11 orders of magnitude, from 1 GeV to 10^{11} GeV, and is described by a power law $\propto E^{-\gamma}$ with two breaks at the ''knee,'' at $\simeq 4 \times 10^{15}$ eV, and at the ''ankle,'' at 5×10^{18} eV. Above the knee the spectrum steepens from a power law index $\gamma \simeq 2.7$ to $\simeq 3.2$. Above the ankle the spectrum flattens again to a power law index $\gamma \simeq 2.8$. Cosmic rays with energies above the ankle cannot be confined by the galactic magnetic field, and the lack of counterparts in our Galaxy suggests that the ankle marks a crossover from a galactic component to a component of extra-galactic origin. Data from the Fly's Eye experiment also suggest that the chemical composition is dominated by heavy nuclei up to the ankle and by protons beyond [3].

If UHECR have an extra-galactic origin, we would expect a cutoff in the spectrum due to the fact that in the bottom-up scenario UHECR are assumed to be protons accelerated in powerful astrophysical sources: Even if they can achieve, under extreme conditions, such high energies, they will lose their energy mostly by pion production on the microwave background. For sources further away than a few dozen Mpc this would predict a break in the cosmic ray flux known as the Greisen-Zatsepin-Kuzmin (GZK) cutoff [4], around 50 EeV. This break has not been observed by experiments such as Fly's Eye [3], Haverah Park [5], Yakutsk [6], Hires [7] and AGASA [8], which instead show an extension beyond the expected GZK cutoff and events above 100 EeV.

One of the possible solutions to the lack of observed counterparts to the highest energy events [9,10] is to suppose the existence of large scale intervening magnetic fields with intensity $B \sim 0.1-1\ \mu$G [10], which would provide sufficient angular deflection even for high energies and could explain the large scale isotropy of arrival directions observed by the AGASA experiment [8] as due to diffusion.

It has been realized recently that magnetic fields as strong as $\simeq 1\ \mu$G in sheets and filaments of large scale structures, such as our Local Supercluster, are compatible with existing upper limits on Faraday rotation [11–13].

In our previous paper [14] we considered the effects of such strong magnetic fields in the particular case of a single source corresponding to Centaurus A, which is a radiogalaxy located in the southern hemisphere at a distance of 3.4 Mpc. There we employed detailed numerical simulations for the energy spectrum and the angular distribution of ultrahigh energy nucleons propagating in extra-galactic magnetic fields of rms strength between 0.3 and 1 μG. We found that this model is inconsistent with the data when $B \simeq 0.3\ \mu$G because the angular distribution predicted is not isotropic but concentrated around the position of the source and because the northern hemisphere experiments should never have detected the highest energy events for which the angular deflection is too weak to bring the particle in the field of view of these experiments; therefore we argued that at least a few sources within the GZK cutoff are required to produce the observed UHECR flux.

The goal of our present paper is to elaborate more detailed constraints on the number of sources necessary to reproduce the observed distribution of events above the GZK cutoff, as a function of the poorly known strength of the extra-galactic magnetic field in our Local Supercluster. As will be explained below in more detail, we assume a discrete distribution of sources in the Local Supercluster permeated by magnetic fields of strength up to $B \sim 0.3\ \mu$G and we restrict

ourselves to events above 4×10^{19} eV. We further assume that all sources emit with comparable power and spectrum which do not change significantly on the time scale of UHECR propagation which can be up to a few gigayears for the magnetic fields considered here.

As in our previous paper, we restrict ourselves to UHECR nucleons, and we neglect the galactic contribution to the deflection of UHECR nucleons since typical proton deflection angles in galactic magnetic fields of several μG are $\lesssim10°$ above 4×10^{19} eV [15,16], and thus are small compared to deflection in $\gtrsim0.3$ μG fields extended over megaparsec scales.

As statistical quantities used to test various scenarios we adopt the angular power spectrum based on the set of spherical harmonics coefficients a_{lm}, as used in Ref. [17], which is sensitive to anisotropies on large scales, and the two-point correlation function as defined in Ref. [18], which contains information on the small scale anisotropy.

As will become apparent, the statistics for these quantities is so far limited by the small number of observed events but the present development of large new detectors will considerably decrease their statistical uncertainties. In particular, the Pierre Auger experiment [19] will combine ground arrays measuring lateral shower cross sections with fluorescence telescopes measuring the longitudinal shower development. Since two of these hybrid detectors are planned, one in the southern hemisphere currently under construction in Argentina, and one in the northern hemisphere, full sky coverage will be achieved, with an exposure that is practically uniform in right ascension, and a geometrical dependence on declination. There are, furthermore, plans for space-based air shower detectors such as OWL [20] and EUSO [21] which may also achieve full sky coverage. For this reason it is feasable to consider a multipole analysis of the angular distribution which involves statistical estimators of integrals covering the full sky: Since these estimators involve factors $1/\omega_i$, where ω_i is the exposure associated with the ith observed direction, they are undefined if the exposure vanishes anywhere on the sky. However, even in the absence of full-sky coverage one can define analogous quantities and their estimators (which are then different from the usual spherical multipoles) by simply restricting them to the area of the sky where the exposure function does not vanish. We will use these modified statistical quantities to compare model predictions with the existing AGASA data.

The autocorrelation analysis provides information about the small scale anisotropy and can be applied to partial sky coverage such as for the AGASA experiment without restriction. The observed data actually show significant small-scale angular clustering (five doublets and one triplet within 2.5° out of 57 events above 40 EeV). This clustering has a chance probability of less than 1% in the case of an isotropic distribution. It has been pointed out that in the presence of turbulent extra-galactic magnetic fields of fractions of a micro-Gauss clustering could be induced by magnetic lensing [22–25]. The autocorrelation analysis presented in the present paper will demonstrate that quantitatively.

The paper is organized as follows: in Sec. II we briefly describe our numerical simulations, in Secs. III and IV we present our results on multipole analysis and autocorrelation function, respectively. Section V briefly reconsiders Centaurus A as the unique source in case of a field as strong as a micro-Gauss and in Sec. VI we conclude.

II. NUMERICAL SIMULATIONS

We use the same numerical approach used in earlier publications [14,23,24], but we take a discrete distribution of sources centered at 20 Mpc from Earth and distributed on a sheet with a Gaussian profile of thickness 3 Mpc and radius 20 Mpc, with the source density following the profile of the sheet and no sources present within 2 Mpc from the observer. This is a simple approximation to our location in the Local Supercluster and to its shape. The magnetic field characteristics are assumed to be constant on the length scales of interest. We also assume that the sources inject protons with an E^{-2} spectrum extending up to $\simeq10^{21}$ eV. We note that the angular distributions are not very sensitive to assumptions on the injection spectrum.

We assume a random turbulent magnetic field with power spectrum $\langle B(k)^2\rangle\propto k^{n_B}$ for $2\pi/L<k<2\pi/l_c$ and $\langle B^2(k)\rangle=0$ otherwise. We use $n_B=-11/3$, corresponding to Kolmogorov turbulence, in which case L, the largest eddy size, characterizes the coherence length of the magnetic field. For the latter we use $L\simeq1$ Mpc, corresponding to about one turn-around in a Hubble time. Physically one expects $l_c\ll L$, but numerical resolution limits us to $l_c\gtrsim0.008L$. We use $l_c\simeq0.01$ Mpc. The magnetic field modes are dialed on a 64^3 grid in momentum space according to this spectrum with random phases and then Fourier transformed onto the corresponding grid in location space. The rms strength B is given by $B^2=\int_0^\infty dk\,k^2\langle B^2(k)\rangle$.

Typically, 5000 trajectories are computed for each realization of the magnetic field obtained in this way and of the source positions, for 10–20 realizations in total. Each trajectory starts at a source randomly chosen from the fixed list of the realization, corresponding to equal power of all sources. Only those trajectories that cross a sphere of 1.75 Mpc radius around Earth (corresponding to 5° viewed from 20 Mpc distance) are used. Each time such a trajectory crosses this sphere, arrival direction and energy are registered as one event. Each trajectory is followed for a maximal time of 10 Gyr and as long as the distance from the center of the Local Supercluster is smaller than 40 Mpc. The results do not significantly depend on these cutoffs. Furthermore, the distance limit is reasonable physically as it mimics a magnetic field concentrated in the large scale structure, with much smaller values in the voids, as generally expected. Similar codes have been developed in Refs. [26].

When dialing simulated data sets from the simulated sky distributions, one has to take into account the non-uniform exposure of the particular experiment considered. This can be done by dialing from the simulated distribution multiplied by an exposure function depending on the sky solid angle Ω. This function, measured in units of km^2 years, gives the effective time-integrated collective area of the detector in a given direction Ω. A detector which operates continuously will have an exposure function roughly independent of right

ascension and thus will only depend on the declination angle δ. We will only need the exposure function up to an irrelevant overall normalization. For a detector at a single site we use the following parametrization:

$$\omega(\delta) \propto \cos a_0 \cos\delta \sin\alpha_m + \alpha_m \sin a_0 \sin\delta, \tag{1}$$

where a_0 is the latitude of the detector and α_m is zero for $\xi > 1$, π for $\xi < -1$, and $\cos^{-1}(\xi)$ otherwise, where $\xi \equiv (\cos\theta_m - \sin a_0 \sin\delta)/[\cos a_0 \cos\delta]$. The angle θ_m is the maximal zenith angle out to which the detector is fully efficient (60° for Auger, 45° for AGASA). The exposure function which results for the AGASA experiment and that we will use in the following, has been discussed, for example, in Ref. [27], see in particular Fig. 2 there.

III. THE ANGULAR POWER SPECTRUM

The angular power spectrum is defined as the average a_{lm}^2:

$$C(l) = \frac{1}{2l+1} \sum_{m=-l}^{l} a_{lm}^2, \tag{2}$$

and the statistical estimator for the spherical harmonic coefficients a_{lm} is given by [17]

$$a_{lm} = \frac{1}{\mathcal{N}} \sum_{i=1}^{N} \frac{1}{\omega_i} Y_{lm}(u^i), \tag{3}$$

where N is the number of discrete arrival directions, either of the real data or randomly sampled from the simulated sky distributions. Furthermore, ω_i is the total experimental exposure at arrival direction u^i, $\mathcal{N} = \Sigma_{i=1}^{N} 1/\omega_i$ is the sum of the weights $1/\omega_i$, and Y_{lm} is the real-valued spherical harmonics function.

In order to obtain the statistical distribution of the $C(l)$ predicted by specific simulated scenarios, we dial $C(l)$ typically 10^4 times from the simulated distributions [multiplied by the exposure function $\omega(\delta)$] for each realization of the magnetic field and the source positions.

For each l we plot the average over all trials and realizations as well as two error bars. The smaller error bar (shown to the left of the average) is the statistical error, i.e. the fluctuations due to the finite number N of observed events, averaged over all realizations, while the larger error bar (shown to the right of the average) is the ''total error,'' i.e. the statistical error plus the cosmic variance, or in other words, the fluctuations due to a finite number of events and the variation between different realizations of the magnetic field and source positions.

To estimate the true power spectrum from Eqs. (2) and (3) requires data with full sky coverage and therefore at least two detector sites such as forseen for the Auger experiment. For its exposure function we add Eq. (1) for two sites located at $a_0 = -35°$ and at $a_0 = 39°$. The AGASA experiment only has partial sky coverage and, consequently, the true multipole spectrum cannot be computed from its data. For this case we consider the quantities defined by restricting Eq. (3) to the sky area where $\omega(\delta) > 0$. This method is also used in the analysis of cosmic microwave background fluctuations where window functions are used which are unity in the observed region and zero elsewhere. In our case this corresponds to using the AGASA exposure function for the ω_i in Eq. (3) for the coefficients a_{lm}. This defines the modified angular power spectrum $C(l)$ both for the simulated data sets and the real data.

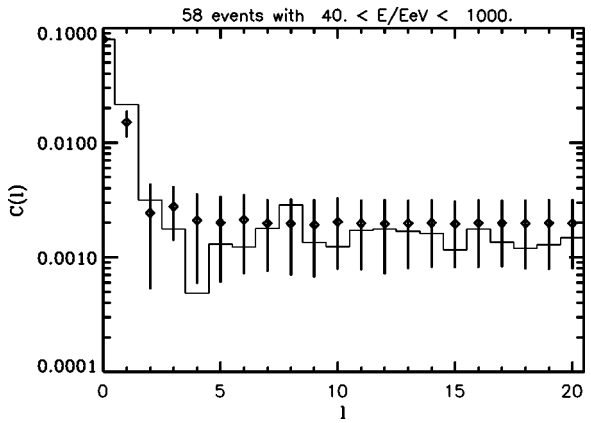

FIG. 1. Comparison of the angular power spectrum $C(l)$, Eqs. (2), (3), resulting from the $N = 58$ events above 40 EeV observed by AGASA (histogram), with the one predicted for an isotropic distribution (diamonds with error bars representing the statistical error), as a function of multi-pole l.

We start by comparing in Fig. 1 the power spectra predicted by the completely isotropic distribution with the AGASA exposure function with the actual AGASA results which appear completely consistent with isotropy on large scales. Note that the increasing power for $l = 0$ and $l = 1$ is due to the incomplete sky coverage of AGASA.

In the following figures, in case of full sky coverage, we show as a solid line the analytical prediction for an isotropic distribution. In this case the power is the same for all l values and decreases as $1/N$ as the number of arrival direction increases. AGASA data are shown as histograms. A pure monopole intensity distribution is equivalent to isotropy while the strength of other multipoles relative to the monopole is a measure of anisotropy.

Since the typical experimental angular resolution is $\simeq 3°$, in principle information is contained in modes up to $l \sim 60$. In the following we show the values of $C(l)$ with l only up to 10 because the structure on small scales corresponding to larger l is better described by the autocorrelation function discussed in the next section.

In Figs. 2 and 3, we compare the angular power spectrum $C(l)$ predicted for the AGASA experiment at energies $E \geqslant 40$ EeV, for magnetic field strength $B = 0.05\ \mu$G, and 100 and 400 sources, respectively, with the actual AGASA data. Both plots have been obtained for $N = 58$, the present number of events with energies above 4×10^{19} eV observed by AGASA.

The case of 100 sources seems roughly consistent with the experimental data while the case of 400 sources shows some deviations for the lowest multipoles. This can be interpreted as the magnetic field being too weak to sufficiently

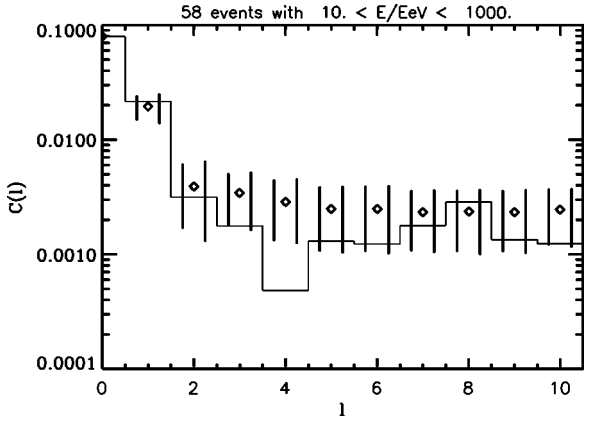

FIG. 2. The angular power spectrum $C(l)$, Eqs. (2), (3), as a function of multipole l, obtained for the AGASA exposure function for $N=58$ events observed above 40 EeV, sampled from 20 simulated realizations for $B=0.05$ μG with 100 sources in the Local Supercluster. The diamonds indicate the realization average, and the left and right error bars represent the statistical and total (including cosmic variance due to different realizations) errors, respectively; see text for explanations. The histogram represents the AGASA data.

isotropize the arrival directions with respect to the sources which were assumed to follow the Local Supercluster: For a number of sources much larger than the number of observed events N, it is likely that each observed event has been produced by a different source. The number of contributing sources is thus maximal and the fluctuations around the assumed (nonisotropic) distribution is minimal, making the anisotropy more visible. This is illustrated by Fig. 4, which shows the UHECR angular distribution as seen on Earth in terrestrial coordinates for $E \geqslant 40$ EeV, $B=0.05$ μG, and 400 sources. The distribution is concentrated around the solid line which represents the supergalactic plane.

In contrast, the scenario with 100 sources seems to be more sensitive to the limited statistics due to the relatively small number of events observed by AGASA. In fact, the statistical errors due to the small number of events at low multipoles are higher in Fig. 2 than in Fig. 3.

For the full sky exposure function corresponding to the Auger parameters, and assuming 500 oberved events, we obtain the situation shown in Fig. 5. In this case the deviation from isotropy, plotted as the solid line, is much more evident and would be easily determined by future observations. As we will show and explain in the next section, the scenario with 100 sources is, however, ruled out by the AGASA data from the analysis of the autocorrelation function. For the relatively small deflection induced by $B=0.05$ μG, the number of sources must be at least as large as the number of events observed in different directions; much fewer than 100 sources are therefore ruled out in this case.

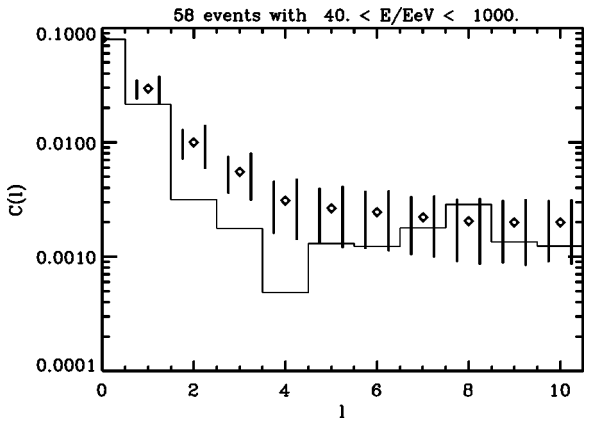

FIG. 3. Same as Fig. 2, but for 400 sources.

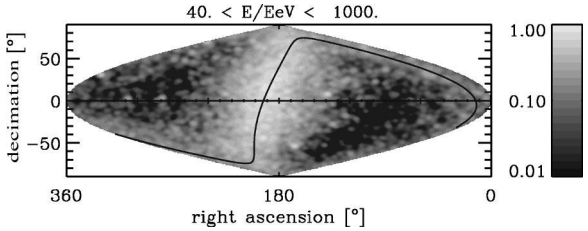

FIG. 4. The angular image in terrestrial coordinates, averaged over all 20 magnetic field realizations of 5000 trajectories each, for events above 40 EeV, as seen by a detector covering all Earth with $B=0.05$ μG and 400 sources. The gray scale represents the integral flux per solid angle. The solid line marks the supergalactic plane. The pixel size is 1° and the image has been convolved to an angular resolution of 2.4° corresponding to AGASA.

We now investigate whether stronger magnetic fields, by providing larger angular deflection, might provide a better match to isotropy. In particular, we focus on the case where $B=0.3$ μG. In Fig. 6 we show results for $B=0.3$ μG and 10 sources, all other assumptions being the same as in Fig. 2.

The distribution seems to be roughly consistent with the data, but we also found that 5 and 100 sources result in almost the same distribution. Since in this case the limited statistics does not allow us to discriminate between widely different number of sources, we turn to the case of Auger exposure with full sky coverage, assuming 500 events observed above 40 EeV. The results are shown in Fig. 7 and

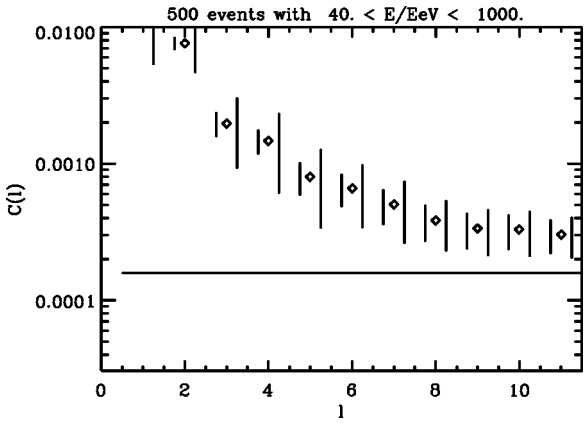

FIG. 5. The angular power spectrum $C(l)$, Eqs. (2), (3), as a function of multipole l, obtained for the Auger exposure function, assuming $N=500$ events observed above 40 EeV, sampled from 20 simulated realizations for $B=0.05$ μG with 100 sources in the Local Supercluster. Average and error bars are as in Fig. 2. The solid line represents the analytical prediction for an isotropic distribution.

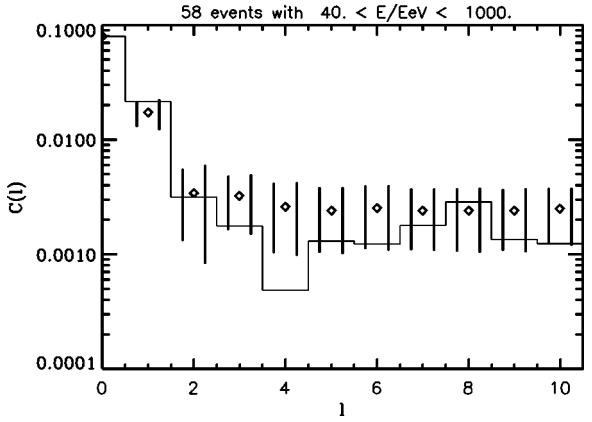

FIG. 6. Same as Fig. 2, but for $B=0.3$ μG and 10 sources.

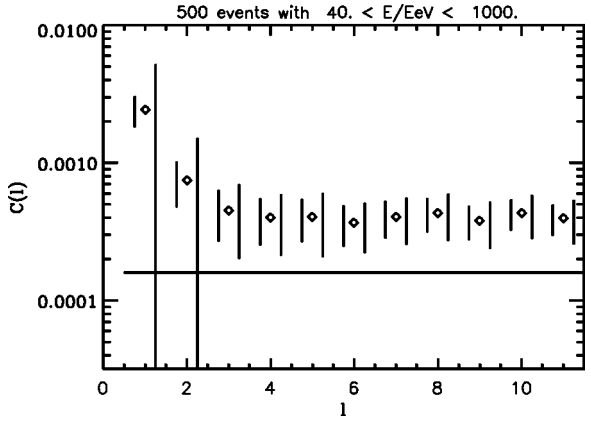

FIG. 8. Same as Fig. 5, but for $B=0.3$ μG and 10 sources.

Fig. 8 for the case for 5 and 10 sources, respectively. The case of 100 sources is already ruled by the autocorrelation function of the AGASA data, as will be shown in the next section.

Note that as for the weak field case the scenarios shown in Figs. 7 and 8 predict an anisotropy that should be easily detectable by the Pierre Auger experiment, in contrast to the AGASA experiment (compare Fig. 6). More generally, we note that the scenario with $B=0.05$ μG gives a distribution very different from the one with $B=0.3$ μG. Thus future experiments with full sky coverage should be able to give important information on the strength of the magnetic field in the Local Supercluster by performing a multipole analysis. Furthermore, in the present case of $B=0.3$ μG Figs. 7 and 8 show that multipoles $l\gtrsim 3$ hardly depend on the number of sources, whereas the lowest multipoles, which are less influenced by deflection, have a noticeable dependence on the number of sources, similarly to the case of weak field $B \lesssim 0.05$ μG.

If a nearly isotropic angular distribution is confirmed by future observations, we can conclude that for magnetic fields $B\simeq 0.3$ μG a number of sources of 5–10 would be favored by the data. As will be shown in the next section, the autocorrelation function does not allow a much higher number of sources because magnetic lensing would not produce sufficient clustering on small scales. On the other hand, much fewer than 5 sources are ruled out by the arguments given in our previous paper [14].

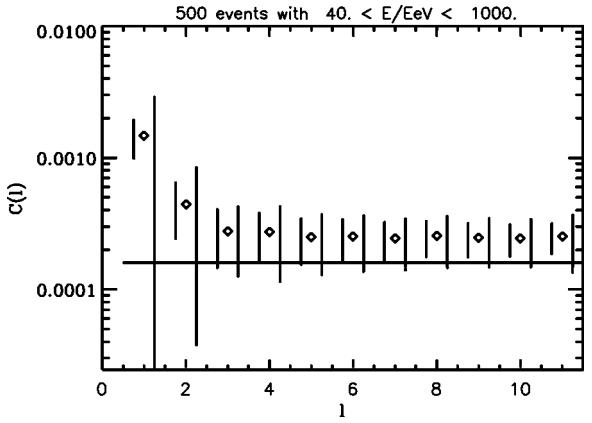

FIG. 7. Same as Fig. 5, but for $B=0.3$ μG, 5 sources, and 20 realizations.

Assuming an energy independent exposure function and using a simple E^{-2} spectrum, it is possible to estimate the number of events which will be observed in the future. In the case of Auger observatories, for a total acceptance of $\simeq 7000$ km^{2}sr per array, in five years we should observe ~ 2200 events above 4×10^{19} eV [17]. Here we have been conservative and used $N=500$.

IV. AUTOCORRELATION FUNCTION

For the autocorrelation function we follow the same approach used in Ref. [18]. We start from either actual data or from a randomly generated set of N events dialed from the simulated distributions, multiplied by the exposure function. For each event we divide the sphere into concentric bins with a fixed angular size $\Delta\theta$, and we count the number of events falling into each bin. We then divide by twice the solid angle size $S(\theta)$ of the corresponding bin, arriving at

$$N(\theta)=\frac{1}{2S(\theta)}\sum_{j\neq i} R_{ij}(\theta), \tag{4}$$

where

$$R_{ij}(\theta)=\begin{cases} 1 & \text{if } \theta_{ij} \text{ is in same bin as } \theta, \\ 0 & \text{otherwise.} \end{cases}$$

We note that the autocorrelation function in the strict sense would include a factor $(\mathcal{N}^2\omega_i\omega_j)$ under the sum in Eq. (4). However, the differences are small and in any case we are free to choose any statistical quantity as long as the same quantity and its fluctuations are used to compare simulations and data.

In analogy to the preceding section, for each magnetic field and source position realization we dial $N(\theta)$ 10^4 times from the simulated distributions in order to obtain its average and variances for which we plot the same two error bars as for the power spectrum. The histograms shown subsequently represent again the result for the AGASA data, where the sharp peak at small separation angles results from the six

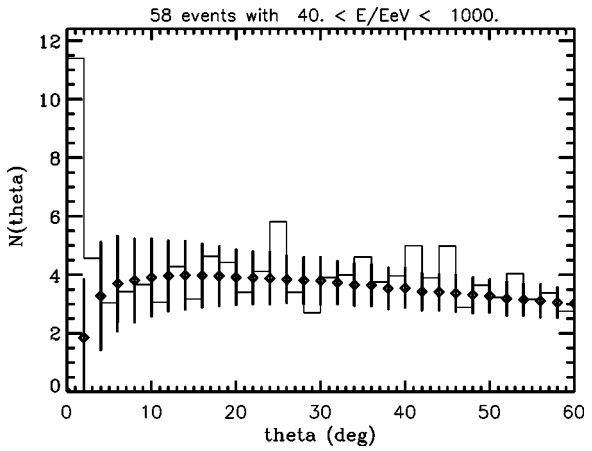

FIG. 9. Comparison of the angular correlation function $N(\theta)$, Eq. (4), resulting from the $N=58$ events above 40 EeV observed by AGASA (histogram), with the one predicted for an isotropic distribution (diamonds with error bars representing the statistical error) as a function of angular distance θ. A bin size $\Delta\theta=2°$ was used.

observed clusters. We have verified that using incorrect exposure functions in general destroys the agreement found between a simulated isotropic distribution and the data at large θ [8]. The observed distribution of events thus reflects the non-uniform exposure [27,28].

We start by comparing the autocorrelation function for the real AGASA data with the isotropic distribution in Fig. 9. This demonstrates that the AGASA data are completely consistent with isotropy except at scales larger than a few degrees.

In Fig. 10 we show the angular correlation function for $N=58$ events with energies $E\geqslant 40$ EeV, predicted by simulations with $B=0.05$ μG and 100 sources, using the AGASA exposure function.

This case shows no correlation at angles as small as the angular resolution, where AGASA shows a peak, whereas

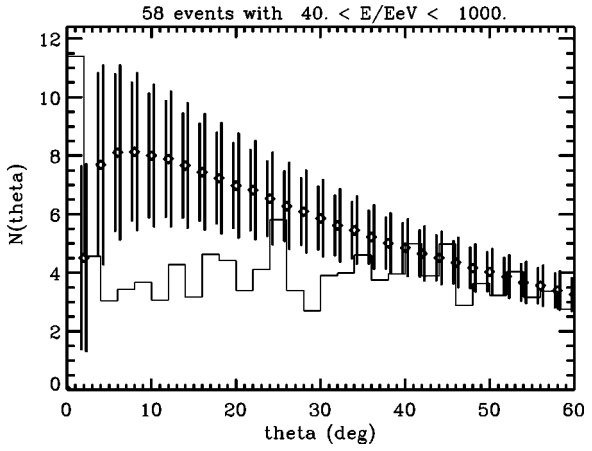

FIG. 10. The angular correlation function $N(\theta)$, Eq. (4), as a function of angular distance θ, obtained for the AGASA exposure function, for $N=58$ events observed above 40 EeV, sampled from 20 simulated realizations for $B=0.05$ μG with 100 sources in the Local Supercluster. Average and error bars are as in Fig. 2. The histogram again represents the AGASA data. A bin size $\Delta\theta=2°$ was used.

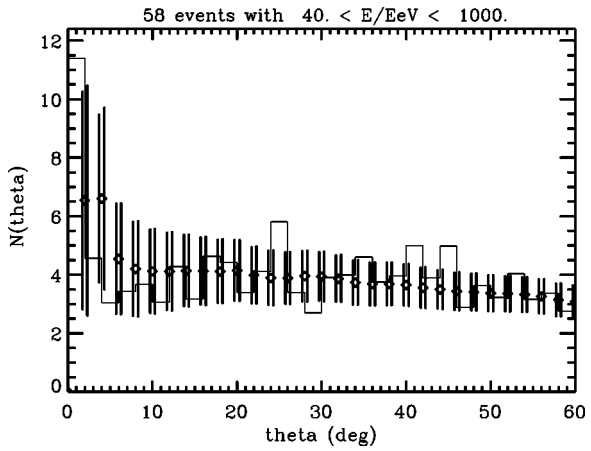

FIG. 11. Same as Fig. 10, but for $B=0.3$ μG and 5 sources with 20 realizations.

there are strong correlations at larger angles, which is not consistent with the observed isotropic distribution at large scales. This also corresponds to the fact that in the case of weak magnetic fields we expect that clusters just reflect the point-like sources but if the number of sources is much larger than the number of observed events N, each source contributes at most one event and clustering is not possible. As remarked in the preceding section, a much smaller number of sources is not possible either due to the large number of observed arrival directions.

In Figs. 11, 12, and 13 we show the angular correlation functions predicted by scenarios with $B=0.3$ μG, with 5 and 10 and 100 sources, respectively. In the case of 100 sources the simulated distribution does not show any correlation at small scales. Similarly to the weak field case, this can be understood due to the fact that the source images produced by magnetic lensing contain at most one event if the number of sources is much larger than N. Note also that cosmic variance becomes very small for $N\gtrsim 100$. We obtain the same result for $B=0.1$ μG and 100 sources. Thus we can argue that 100 is an approximate current upper limit for the number of sources. On the other hand for 5–10 sources the simulated autocorrelation function seems to be in agreement with the observed clustering at small scales.

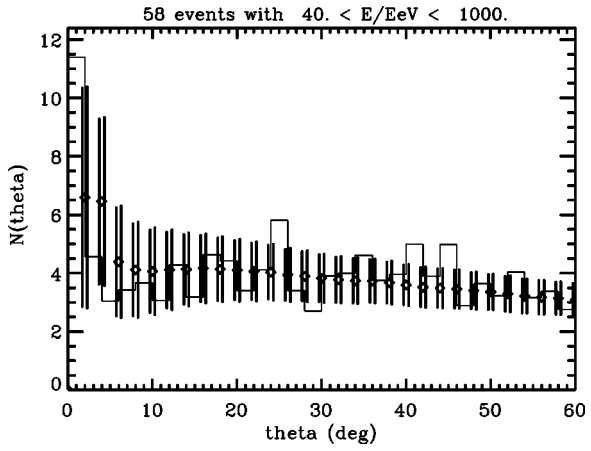

FIG. 12. Same as Fig. 10, but for $B=0.3$ μG and 10 sources.

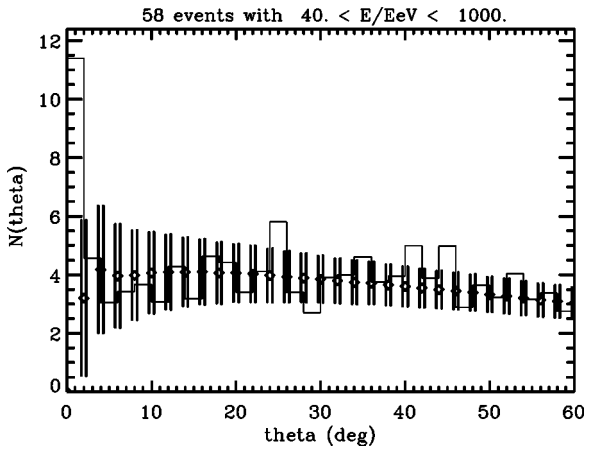

FIG. 13. Same as Fig. 10, but for $B=0.3$ μG and 100 sources with 18 realizations.

Figure 14 shows that the spectrum is also consistent with the data in this case. Note that the spectrum is steeper than the injection spectrum ($\propto E^{-2}$) at low energies, while the two match at high energies. This results from an increased local residence time due to diffusion at low energies and rectilinear propagation (hence unaffected energy spectrum) at high energies [23]. We note in this context that sources outside our Local Supercluster do not contribute significantly to the observable flux in out context with sources residing in magnetized clusters and superclusters: For particles above the GZK cutoff this is because sources outside the Local Supercluster are beyond the GZK distance. Sub-GZK particles are mainly contained in the magnetized environment of their sources as discussed above and thus exhibit a much higher local overdensity than their sources. Further, the suppressed flux of low energy particles leaving their environment is largely kept out of our Local Supercluster by its own magnetic field. This can be seen in Fig. 15 which shows the observable flux resulting from an $E^{-2.4}$ spectrum isotropically impinging from outside onto a sphere at 40 Mpc around

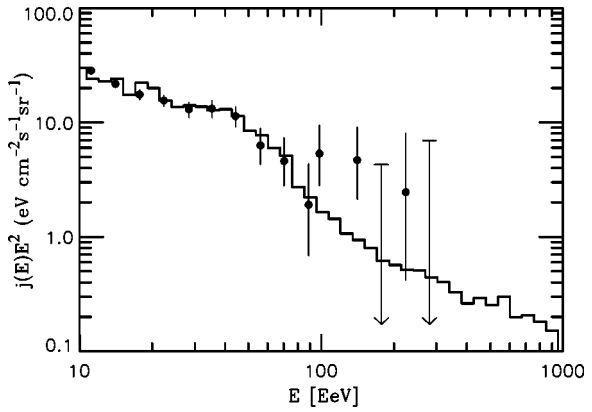

FIG. 14. The realization averaged energy spectrum obtained for the AGASA exposure function for the case with $B=0.3$ μG and 10 sources injecting protons with an E^{-2} spectrum up to 10^{21} eV, corresponding to Figs. 8 and 12. The solid line represents the spectrum that would have been detected by AGASA. The one sigma error bars indicate the AGASA data.

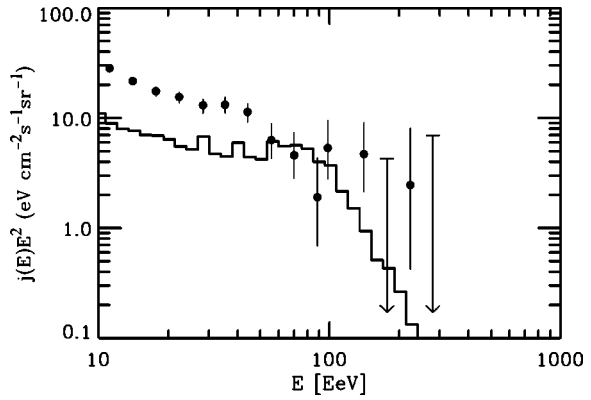

FIG. 15. The unnormalized, solid angle averaged energy spectrum observed at Earth resulting from a $E^{-2.4}$ isotropic proton flux arriving at a sphere of 40 Mpc around the Local Supergalactic center with a field following the Local Supercluster profile of maximum strength $B=0.3$ μG. The steeper spectrum as compared to the E^{-2} injection spectrum assumed in the simulations with local sources mimics the increasing energy loss length with energy.

the center of our supercluster, this time conservatively assuming a magnetic field scaling with the sheet profile (the effect would be even stronger for a more extended field). Note that despite the smaller energy losses the sub-GZK particles arriving from outside the Local Supercluster are likely to have a more strongly suppressed spectrum at low energies due to their containment in the source region, and thus cannot contribute significantly to the observed flux. A significant contribution from large distance sources would require magnetic fields in the nano-Gauss range, and even then would be unlikely to explain the observed clustering.

In Fig. 16 we show the autocorrelation function expected for Auger exposures for $B=0.3$ μG and 10 sources. This demonstrates that, for the amount of data expected with next generation experiments, the statistics will be dominated by cosmic variance instead of the limited number of events observed, as is presently the case.

We finally would like to comment on the dependence of our results on the largest eddy size L and the magnetic power law index n_B for values different from the ones used in this

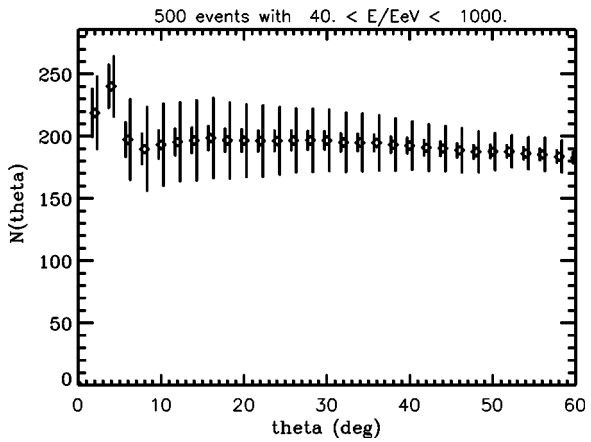

FIG. 16. Same as Fig. 12, but obtained for the Auger exposure function, assuming $N=500$ events observed above 40 EeV.

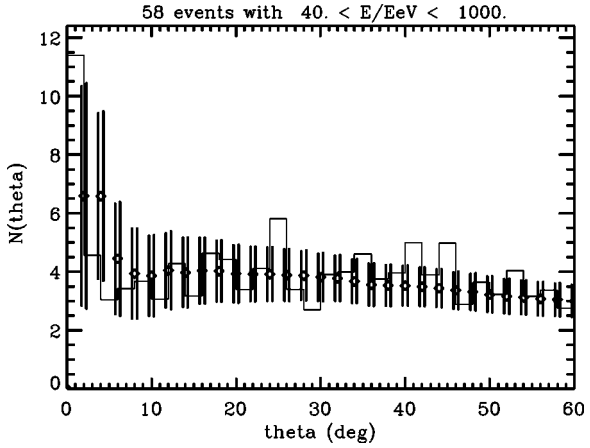

FIG. 17. The same as Fig. 13 but for 9 realizations and magnetic power law index $n_B=-2.5$.

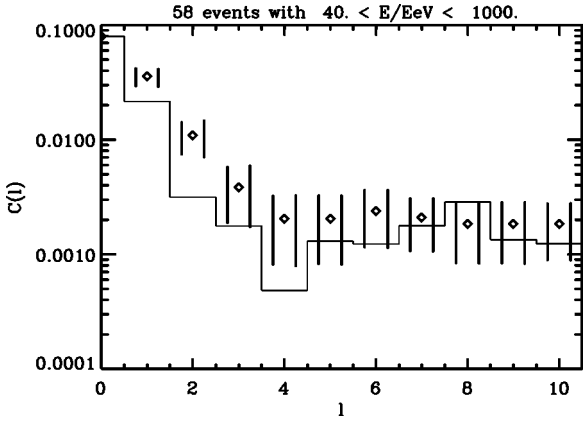

FIG. 18. Same as Fig. 2, but for the scenario with Centaurus A at 3.4 Mpc distance as the single source, a field of 1 μG, and 20 realizations.

work, $L=1$ Mpc and $n_B=-11/3$. These values are well motivated but do not necessarily reflect the actual situation. The predicted large scale UHECR distribution is not very sensitive to these values as long as most power is on the largest scales, i.e. $n_B \geqslant -3$ and the average deflection angle $\propto B\lambda_c^{1/2}$ is held constant, where λ_s is the coherence scale of the field [23]. However, the angular correlation function can be significantly influenced by the small scale structure of the magnetic field. This is demonstrated in Fig. 17, where we plot the autocorrelation function for the case with 100 sources and $B=0.3$ μG for a simulation with $n_B=-2.5$. In this case the magnetic field has more power on small scales which are cut off at $l_c \simeq 0.01$ Mpc in our simulations. This leads to a stronger effect of magnetic lensing and in turn to increased clustering at small scales as compared to Fig. 13 for a Kolmogorov spectrum. In contrast, the multipole distribution would be hardly distinguishable between $n_B=-11/3$ and $n_B=-2.5$ in this case.

V. ONLY ONE SOURCE: CENTAURUS A

Now we briefly reconsider the model discussed in our previous paper [14], with Centaurus A as single source, and $B=1$ μG. The predictions for the angular power spectrum and the autocorrelation function are compared with the AGASA data in Figs. 18 and 19, respectively.

The angular power spectrum shows a $\simeq 3\sigma$ deviation from the data at $l=2$. Furthermore, the autocorrelation function does not show significant correlations at angular resolution scales, in contradiction to the data. This is due to the fact that for a magnetic field as strong as 1 μG, we are in a range of energies where many overlapping images of the source are produced [25]. Correlations up to relatively large scales would only appear at energies above $\simeq 10^{20}$ eV, as can be seen in Fig. 20 which was produced for the Auger exposure function.

VI. DISCUSSION AND CONCLUSIONS

In the present work we assumed a discrete distribution of continuously emitting sources distributed in the Local Supercluster and estimated the number of sources necessary to reproduce the experimental data on cosmic rays above 4×10^{19} eV, in dependence on the typical strength of the extra-galactic magnetic fields permeating the Local Supercluster. As statistical quantities for this analysis we used spherical multipoles and the autocorrelation function. We found that for weak magnetic fields $\lesssim 0.05$ μG the simulation predictions appear to be not consistent with the observed distribution for any number of sources because the magnetic field is too weak to isotropize the anisotropic distribution associated with the supergalactic plane. Full sky experiments of the size of the Pierre Auger project will be sensitive to the difference in the distribution of multipoles between weak and strong magnetic fields, which thereby could give direct information about the strength of the magnetic fields. For stronger magnetic fields $\simeq 0.3$ μG we found that the number of sources is constrained. In our previous paper [14] we already showed that a single source cannot reproduce the observed isotropic distribution. Here we found that for $\gtrsim 100$ sources the autocorrelation function does not reproduce the correlations observed at small scales. This can be interpreted

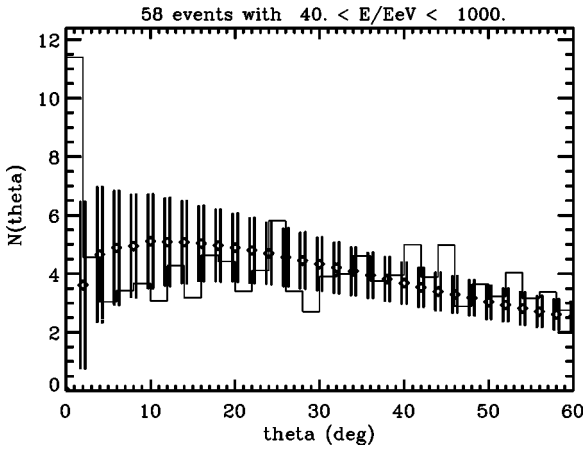

FIG. 19. Same as Fig. 10, but for the scenario with Centaurus A at 3.4 Mpc distance as the single source, a field of 1 μG, and 20 realizations.

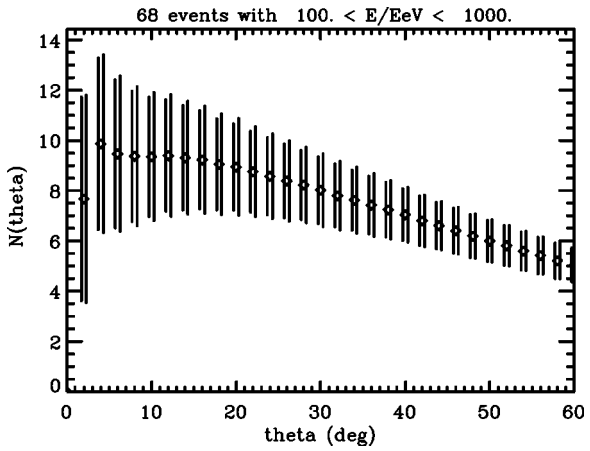

FIG. 20. The angular correlation function $N(\theta)$ as a function of angular distance θ, obtained for the Auger exposure function, assuming $N=68$ events observed above 100 EeV for the scenario with Centaurus A at 3.4 Mpc distance as the single source, a field of 1 μG, and 20 realizations. The bin size is again $\Delta\theta=2°$.

by the fact that for a number of sources much higher than the number of observed events there are more source images produced by lensing than observed events and thus clustering is not observable. Therefore, the current upper limit on the number of contributing sources is $\simeq 100$ in this case. On the other hand, a number of sources around 10 seem to reproduce quite well the observed small scale clustering. We also showed that the model with Centaurus A as the only source and very strong fields $\simeq 1\,\mu$G, considered as marginally consistent in our previous paper [14], is not consistent with isotropy at large scales due to a predicted quadrupole deviation from isotropy and because the autocorrelation function is not consistent with the clustering at small scales observed by AGASA. We conclude then that a distribution of $\simeq 10$ sources in the Local Supercluster, with magnetic fields in the sub-micro-Gauss range, could reproduce at least current observations. This is the case for a turbulent Kolmogorov magnetic field spectrum with largest eddy size $L\simeq 1$ Mpc and constant RMS strength on the supercluster scale and a source probability distribution following an idealized Gaussian profile for the Local Supercluster. Magnetic fields with more power on smaller scales mainly seem to increase clustering at small scales. Finally, we have restricted ourselves to magnetic field characteristics uniform on the scales of interest in the present paper. We find that fields only extending a few Mpc away from the supergalactic plane would lead to cosmic ray arrival distributions that are too anisotropic above 4×10^{19} eV.

Our approach can equally be applied to other source distributions and magnetic field scenarios. In future work we also plan to apply more realistic magnetic field distributions which could contain components that are coherent on scales of several Mpc. Such distributions can be obtained, for example, from large scale structure simulations which include magnetic fields. Application to non-continuous or bursting sources is also possible.

Due to the still sparse statistics of current data, in the present paper we refrained from quantifying the statistical significance of deviations between models and data, because small number fluctuations are in general not Gaussian and, for different multipoles and separation angles, can be correlated. Results based on comparison with the AGASA data presented here should rather be understood as suggestive tendencies. Quantitative significances can be obtained by determining in how many simulated trials a certain quantity, such as the multipoles and autocorrelations studied here, or certain combinations thereof, show deviations from the data of opposite sign to the average deviation. We leave that to a study with data of much higher statistics above $\simeq 10^{19}$ eV than available today, as expected from future full-sky experiments. These experiments will put much more stringent constraints both on the number of sources and the magnetic field strength.

ACKNOWLEDGMENTS

We thank Martin Lemoine for past and ongoing collaborations related to the development of numerical propagation codes. C.I. also wishes to thank Olivier Doré and Lorenzo Sorbo for useful suggestions on the manuscript.

[1] For recent reviews see J.W. Cronin, Rev. Mod. Phys. **71**, S165 (1999); P. Bhattacharjee and G. Sigl, Phys. Rep. **327**, 109 (2000); A.V. Olinto, *ibid.* **333**, 329 (2000); X. Bertou, M. Boratav, and A. Letessier-Selvon, Int. J. Mod. Phys. A **15**, 2181 (2000).

[2] See, e. g., P.L. Biermann, J. Phys. G **23**, 1 (1997).

[3] D.J. Bird *et al.*, Phys. Rev. Lett. **71**, 3401 (1993); Astrophys. J. **424**, 491 (1994); **441**, 144 (1995).

[4] K. Greisen, Phys. Rev. Lett. **16**, 748 (1966); G.T. Zatsepin and V.A. Kuzmin, Pis'ma Zh. Éksp. Teor. Fiz. **4**, 114 (1966) [JETP Lett. **4**, 78 (1966)].

[5] See, e. g., M.A. Lawrence, R.J.O. Reid, and A.A. Watson, J. Phys. G **17**, 733 (1991), and references therein; see also http://ast.leeds.ac.uk/haverah/hav-home.html

[6] N.N. Efimov *et al.*, *Proceedings of the International Symposium on Astrophysical Aspects of the Most Energetic Cosmic Rays*, edited by M. Nagano and F. Takahara (World Scientific, Singapore, 1991), p. 20; B.N. Afnasiev, *Proceedings of the International Symposium on Extremely High Energy Cosmic Rays: Astrophysics and Future Observatoires*, edited by M. Nagano (Institute for Cosmic Ray Research, Tokyo, 1996), p. 32.

[7] D. Kieda *et al.*, Proceedings of the 26th ICRC, Salt Lake, 1999; see also http://www.physics.utah.edu/Resrch.html

[8] Takeda *et al.*, Astrophys. J. **522**, 225 (1999); M. Takeda *et al.*, Phys. Rev. Lett. **81**, 1163 (1998); Hayashida, *et al.*, Astrophys. J. **522**, 225 (1999); see also http://www-akeno.icrr.u-tokyo.ac.jp/AGASA/

[9] G. Sigl, D.N. Schramm, and P. Bhattacharjee, Astropart. Phys. **2**, 401 (1994).

[10] J.W. Elbert and P. Sommers, Astrophys. J. **441**, 151 (1995).
[11] J.P. Vallée, Fundam. Cosmic Phys. **19**, 1 (1997).
[12] D. Ryu, H. Kang, and P.L. Biermann, Astron. Astrophys. **335**, 19 (1998).
[13] P. Blasi, S. Burles, and A.V. Olinto, Astrophys. J. Lett. **514**, L79 (1999).
[14] C. Isola, M. Lemoine, and G. Sigl, Phys. Rev. D **65**, 023004 (2002).
[15] G. Medina-Tanco, E.M. DeGouveia Dal Pino, and J.E. Horvath, astro-ph/9707041.
[16] L.A. Anchordoqui and H. Goldberg, Phys. Rev. D **65**, 021302(R) (2002); T. Stanev, Astrophys. J. **479**, 290 (1997).
[17] P. Sommers, Astropart. Phys. **14**, 271 (2001).
[18] P.G. Tinyakov and I.I. Tkachev, JETP Lett. **74**, 1 (2001); M. Takeda *et al.*, Proceedings of ICRC, 2001, p. 345.
[19] J.W. Cronin, Nucl. Phys. B (Proc. Suppl.) **28**, 213 (1992); The Pierre Auger Observatory Design Report, 2nd ed., 1997; see also http://http://www.auger.org/ and http://www-lpnhep.in2p3.fr/auger/welcome.html
[20] D.B. Cline and F.W. Stecker, OWL/AirWatch science white paper, astro-ph/0003459; see also http://lheawww.gsfc.nasa.gov/docs/gamcosray/hecr/OWL/
[21] R. Benson and J. Linsley, Astron. Astrophys. **7**, 161 (1992); see also http://www.ifcai.pa.cnr.it/Ifcai/euso.html
[22] D. Harari, S. Mollerach, and E. Roulet, J. High Energy Phys. **08**, 022 (1999); **02**, 035 (2000); **10**, 047 (2000).
[23] G. Sigl, M. Lemoine, and P. Biermann, Astropart. Phys. **10**, 141 (1999).
[24] M. Lemoine, G. Sigl, and P. Biermann, astro-ph/9903124.
[25] D. Harari, S. Mollerach, E. Roulet, and F. Sanchez, J. High Energy Phys. **03**, 045 (2002).
[26] G. Medina Tanco, astro-ph/9808073; A. Achterberg, Y.A. Gallant, C.A. Norman, and D.B. Melrose, astro-ph/9907060; T. Stanev *et al.*, Phys. Rev. D **62**, 093005 (2000); Y. Ide, S. Nagataki, and S. Tsubaki, astro-ph/0106182.
[27] S. Razzaque and J.P. Ralston, astro-ph/0110045.
[28] P. Tinyakov and I. Tkachev (private communication).